2019 International Conference on Robotics and Automation (ICRA)
Palais des congres de Montreal, Montreal, Canada, May 20-24, 2019

Sleeve Pneumatic Artificial Muscles for Antagonistically Actuated Joints*

Michael F. Cullinan, Conor McGinn, and Kevin Kelly.

Abstract— **Pneumatic artificial muscles (PAMs) have been researched for applications in powered exoskeletons, orthosis and robotics. Their high force to mass ratio, low cost and inherent compliance are particularly advantageous for systems requiring physical interaction with humans.**

Sleeve PAMs, which introduce an internal structure to the actuator, offer improved force capacity, contraction ratio, efficiency and operating bandwidth. In this paper sleeve PAMs are applied to a popular muscle configuration; that of a joint operated antagonistically by two muscles. It is shown that the sleeve PAM can increases the range of joint rotation by 14% or load capacity by over 50% of that of a comparable joint actuated with traditional PAMs, depending on the joint configuration. The stiffness of joints actuated with both PAM types is also studied, particularly the case of closed system operation (mass of air in the PAMs is constant), where the reduced volume of the sleeve PAM significantly increases the observed stiffness. Finally energy consumption is considered, showing substantial savings in the case of joints actuated with sleeve PAMs.

I. Introduction

Safely removing the barriers between man and machine, to facilitate collaborative operation has been a research goal in several areas in recent years. For systems which require the application of large forces, particularly in confined environments or which operate with non-expert users, the need to develop actuation paradigms with excellent safety characteristics is apparent [1]. As any control system has the capacity to fail, actuators which are inherently safe are preferable to those which rely on sensing and control alone to achieve such characteristics [2]. In this regard pneumatic artificial muscles are a promising solution. The use of compressed air as well as the actuators structure ensures inherent compliance, particularly important in constrained impacts [3]. Compliance also has an important physiological effect on users; the ability to manually back drive the system contributing to a feeling of control [4]. This, together with the lightweight nature of these actuators reduces the effective inertia of actuated systems.

While many PAM designs have been proposed [5], the most popular remains the braided or "McKibben" muscle. This consists of a tubular elastic bladder, surrounded by a braid with fibers arranged helically, half clockwise and half counterclockwise (see Fig. 1). The fibers are interwoven to maintain the flexible structure. At each end of this cylinder, solid end-fittings seal the cylinder, allow compressed air into the system and allow fixing of the muscle to the system. The commercially available fluidic muscle developed by Festo operates in an almost identical manner, except the helical fibers are not interwoven and instead are embedded in the bladder material [6]. When compressed air flows into the PAM, the differential pressure across the bladder causes it to expand, pushing out on the braid, tending to expand it radially. As the fibers in the braid are stiff (but flexible) this radial expansion must be accompanied by a longitudinal contraction, and the braid angle (θ in Fig. 1) increases. As the muscle contracts, the force output at a given pressure will reduce due to the increase in braid angle. This is a property of muscle-like actuators; their position/contraction is proportional to a stimulus (in this case differential air pressure). This differs considerably from other actuator types such as electric motors or pneumatic cylinders, where the velocity is controlled by the stimulant (voltage or pressure differential). If the pressure in the muscle is sufficient the helical braid will expand until the braid angle reaches a maximum (theoretically 54.74°) [5], [7].

In practice the braid angle will not reach the theoretical maximum due to friction, bladder elasticity and the force exerted on the end fittings due to the muscle pressure. This latter factor is illustrated in Fig. 1 as the muscle pressure acts not just on the bladder, but also on the end fittings. The force generated acts against the contractile force of the braid, therefore reducing maximum contraction and the force output. The magnitude of the force due to pressure acting on the end fittings is

$$F_{end}=P'A_d \quad (1)$$

where P' is the gauge pressure in the muscle and A_d is the cross sectional area of the end fitting on which the pressure acts. By reducing A_d, the contractile force generated

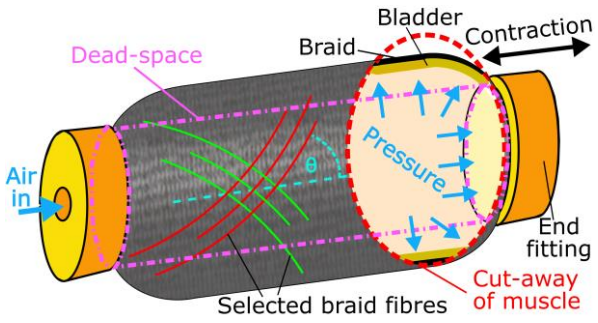

Figure 1. The structure of a PAM

* *M.F. Cullinan is with the Department of Mechanical and Manufacturing Engineering, Trinity College Dublin, Dublin Ireland (phone:35318963767; e-mail: cullinmf@tcd.ie).

C.McGinn., is with the Department of Mechanical and Manufacturing Engineering, Trinity College Dublin, Dublin Ireland (email: mcginnc@tcd.ie)

K.Kelly is with the Department of Mechanical and Manufacturing Engineering, Trinity College Dublin, Dublin Ireland (email: kekelly@tcd.ie)

by the PAM can be increased, thus improving efficiency. Another means by which to increase efficiency is to decrease the volume of the PAM, thereby reducing the mass of air required to achieve the same pressure. This may be achieved by occupying the dead-space (see Fig. 1) of the PAM with a filler material as investigated in [8].

The Sleeve PAM has been proposed to improve efficiency, increase force output and maximum contraction of PAMs by Driver and Shen [9]. In the sleeve PAM (see Fig. 2), a solid internal element extends from where it is rigidly attached to one end fitting, across the dead-space and through the other end fitting (known as the sliding end fitting). Here a pneumatic seal prevents leakage. This reduces the internal volume of the PAM as well as the area of the end fittings over which the muscle pressure acts, thus increasing the force output, maximum contraction and efficiency of the PAM. While the mass of the actuator also increases, the internal element may also be used as a structural component, for example as the upper arm of an elbow being actuated by a sleeve PAM as demonstrated in [10].

The design of the sleeve PAM has subsequently been updated and applied to the McKibben type muscle with distinct bladder and braid [11]. As this actuator was entirely developed in-house, without relying on commercially available PAMs it was possible to remove a greater proportion of the dead-space. Several other features were added such as allowing a load to be applied along the axially central axis (simplifying attachment of the actuator), the repositioning of the sliding pneumatic seal further inside the PAM, thus reducing the possibility of damage to the seal or sliding surface, and the inclusion of a pulley mechanism, changing the contraction/force profile of the actuator while maintaining its external dimensions. This actuator showed an increase in efficiency of up to 48% when compared to the traditional, unaltered PAM, as well as an additional 5% contraction of the PAM. Subsequent testing of dynamic characteristics of the actuator showed up to 120% increase in the bandwidth of the sleeve PAM when compared to a traditional PAM [12]. A phenomenological model, together with an experimentally derived expression for the volume of the PAM and consideration for the mass flow through the valves yielded a dynamic model for the actuator.

There are a number of means by which PAMs may be configured to actuate a joint. For a revolute joint, the fact that PAMs can only impart a tensile force means that some other restoring force is required to operate the joint in the opposite direction. This can be achieved using standard mechanical springs, as in [10], [13], however this means it is impossible to alter the joint stiffness as the spring stiffness is fixed. This capability is desirable in order to alter the dynamics of the system to optimize energy storage (for example during walking) and for safety characteristics, for example maintain low stiffness during high speed traversals and high stiffness when fine control is required. Indeed without the ability to modify joint stiffness it is possible to argue that the low mass property of PAMs is unjustified. In a comparison between electric motors and PAMs, Tavakoli et al. found that electric motors can be lighter than PAMs under most operating conditions [14]. However, controllable joint stiffness is not considered here, and whereas the joint actuated with two PAMs is inherently compliant, achieving same with a joint actuated by an electric motor requires an additional controllable degree of freedom (for example to control the effective length of a spring between the drive train and the joint), hence more mass must be added if this is a requirement.

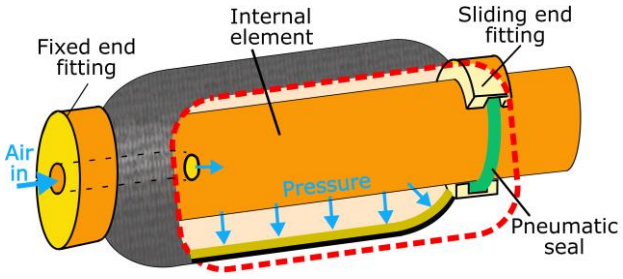

Figure 2. The structure of a sleeve PAM

The contribution of this work is the application of the sleeve PAM to the case of an antagonistically actuated joint. A comparison is made to a joint actuated with traditional PAMs, considering in particular torque, range of rotation, joint stiffness, closed system joint stiffness, damping and energy consumption.

II. Modelling

The phenomenological models of the traditional and sleeve PAMs developed in [12] can be applied to the case of an antagonistically actuated joint. This model represents the PAM as a contractile force, spring and viscous damper in parallel giving the force output as

$$F_{mus}=F_{ce}-Ky-c\dot{y} \quad (2)$$

Where F_{ce} is the contractile force, K is the spring coefficient, c is the viscous damping coefficient and y and $\dot{y}$ are the contraction and contraction velocity respectively. The contractile force is dependent on muscle pressure and the spring force varies with pressure and contraction. Therefore muscle force is given by

$$F_{mus}=A+BP'-(C+DP'+Ey)y-G\dot{y} \quad (3)$$

where P' is the gauge pressure in the PAM, the constants A-E are determined experimentally using static tests, and G is found under dynamic conditions. These constants are specific to the muscle being tested (materials, dimensions, traditional or sleeve).

For an antagonistically actuated joint suing a pulley to transmit the force between the muscles and the joint, the torque output is

$$T=r(F_1-F_2) \quad (4)$$

where r is the radius of the pulley and F_1 and F_2 are the forces exerted by the two PAMs. The contraction of each PAMs can be related to the angle of the joint (β, in radians). Labeling the muscles 1 and 2 this can be expressed as

$$y_1=r\left(\frac{\beta_{range}}{2}+\beta\right), \qquad y_2=r\left(\frac{\beta_{range}}{2}-\beta\right) \quad (5)$$

Here, β_{range} is the total range of rotation of the joint. This range is limited by the maximum extension of the PAMs and is altered by moving the PAM closer to or further from the

pulley. Combining equations 3-5, and assuming that the operating conditions are such that both muscles apply a tensile force, the torque of the joint can be related to β and expressed as:

$$T=r\begin{pmatrix}(P'_1-P'_2)\left(B-Dr\frac{\beta_{range}}{2}\right)\\ -\beta r\left(2C+D(P'_2+P'_1)-2Er\beta_{range}\right)-2G\dot{\beta}r\end{pmatrix} \quad (6)$$

From this it is evident that the joint torque is dependent not just on the pressure in the PAMs but also on joint position. This gives a more complex torque profile than an electric motor. Whereas motors produce the same torque at any point in their rotation and in either direction, due to the reduction in the force exerted by PAMs with contraction, the maximum torque will vary based on the joint position and the direction in which torque is required. At the limits of rotation, the muscle acting to rotate the joint away from the limit will be close to full extension, and hence is capable of large forces in that direction. In contrast the muscle pulling the joint towards the limit is close to full contraction and consequently can only offer a small torque in that direction.

The stiffness of the joint is the derivative of equation 6 with respect to β (without the effect of the damper).

$$\frac{dT}{d\beta}=-r^2\left(2C+D(P'_2+P'_1)+2Er\beta_{range}\right) \quad (7)$$

While the torque is dependent on both the PAM pressures and the joint angle, joint stiffness only depends on the combined pressure in the PAMs. However, as the torque and angle dictate the difference in pressure between the PAMs, the maximum stiffness at an angle is limited by the maximum operating pressure.

III. Testing Apparatus

A detailed account of the test apparatus is given in [12]. This was updated to facilitate testing of an antagonistically actuated joint with the addition of a 80mm diameter pulley attached to the PAMs using 3mm D12 Max 78 Dyneema rope[15]. A CUI AMT203 absolute encoder [16] measured joint position while pressure in the PAMs and the supply pressure was recorded using Honeywell Tru-Stability HSC pressure sensors [17]. STA-1 aluminum S type load cell [18] are attached to each PAM to measure the force they apply. Matrix BX72102C212 2/2 high speed solenoid valves [19] control the flow of compressed air, with inlet and exhaust valves (using multiple valves in parallel for greater flow rate as required) for each muscle. This configuration allows the pressure in each PAM to be controlled independently. The supply pressure for all tests is 500kPA with a maximum muscle operating pressure of 414kPa. For all tests described here the test apparatus operates in a vertical configuration, meaning the mass must be lifted against gravity.

The PAMs (both sleeve and traditional) used in this work have an active length (the distance between the end fittings) of 190mm±2mm. A 40mm internal diameter latex tube with 1.5mm wall thickness forms the bladder, while the braid is composed of PET fibers. The end fittings and internal element are made from aluminum. The characteristics of the PAMs using this combination of materials are given in [12].

The choice of pulley diameter and the point of rotation at which the muscles reach their full extension will alter the operating characteristics of PAM actuated joints. A smaller pulley means that for the same PAM contraction there is greater joint rotation but also a smaller torque. If the PAMs are configured so that when one PAM is at full extension the other is fully contracted, the joint will have a large range of rotation, but relatively low force in the direction of the contracted muscle when compared with a joint where the maximum contraction of the muscles is limited due to the other reaching full extension at a smaller angle. In this work, an 80mm diameter pulley is used for all tests. As an example configuration, the traditional PAMs are arranged so that the joint can rotate by ±0.6rad while maintaining a torque of at least 15Nm in both directions at the limits of rotation at the maximum operating pressure. Two comparable joint configurations using sleeve PAMs are evaluated, both using the same pulley. The first (A), aims to increase the operating range of the joint, while maintaining the torque available across the range of rotation. This is achieved by moving both muscles closer to the pulley. As the sleeve PAM is capable of greater contraction than the traditional PAM this allows the joint to rotate further before reaching the maximum extension of the antagonistic muscle. The second configuration (B) aims to maintain the same range of rotation as the joint actuated with traditional PAMs, but utilize the increased force output of the sleeve PAM to increase torque. Here the sleeve PAMs are positioned so that they reach maximum extension at the same limits of rotation as the traditional PAM.

IV. Joint Torque and Isobaric Stiffness

In order to characterize the torque profile of the joint, the torque which can be applied by each muscle is considered,

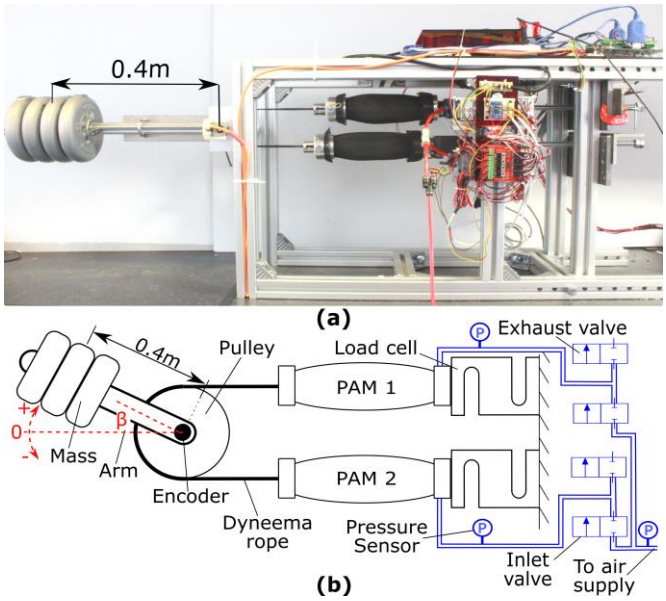

Figure 3. The testing apparatus suporting a mass (a), and shown schematically (b).

using equation 3, at six test pressures. This is shown for both directions of rotation and each joint configuration in Fig. 4. Stretch in the Dyneema cable was accounted for, with testing showing an extension of 0.0017mm/N over the 30 cm length of each cable.

To verify the model experimentally, the arm and mass were removed from the joint so that there is no output torque from the joint. The two PAMs then act against each other only while rotating the joint. The test sequence maintains one PAM at the test pressure while the other PAM's pressure is slowly increased to change the joint position. When both PAMs are at the same pressure (which occurs at 0rads as there is no output torque) their roles reverse and the pressure in the PAM which was maintained at the test pressure is slowly reduced until it reaches atmospheric pressure. The procedure is then repeated in reverse so that the joint rotates back to its original position.

The results of these tests for six test pressures are shown in Fig. 4. The torques represented here are those exerted by the PAM at the test pressure and align with those generated by the model. From this it is seen that in configuration A at the same pressure and position the torque is always equal to or slightly greater than the joint actuated by traditional PAMs while also giving an additional 14% of rotation past the original limits of the joint. For configuration B, the range of rotation is approximately the same as that of the joint actuated using traditional PAMs, while the torque is at least 25% greater, rising to over 50% at the limits of contraction. There is significant hysteresis observed as the joint moves in one direction or the other, with this being more significant for the sleeve PAM configurations. This is likely due to the added friction at the sliding seal.

Maximum isobaric stiffness, as calculated using the joint model is shown in Fig. 4 for each joint configuration. Three different applied torques are considered. While equation 7 shows no dependence of torque or joint angle, the sum of the pressures in the PAMs is limited by the required difference in the PAM pressures to maintain the joint position and torque. For example, when no output torque is required and the joint is at angle 0rad both PAMS can be inflated to their maximum pressure. However, to move from this position one of the PAMs must reduce its pressure thus reducing the joint stiffness. The point in the rotation where maximum stiffness occurs is moved depending on the joint torque, but occurs where both PAMs can be inflated to their maximum pressure.

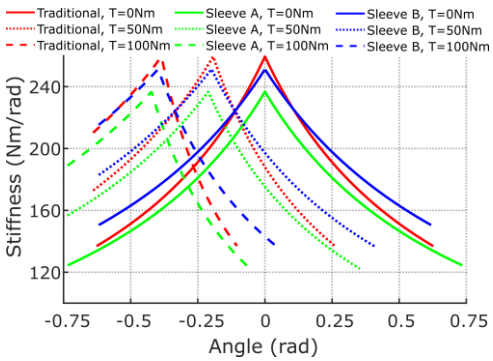

Figure 5. The maximum stiffness of the three joint configurations with three different output torques as modelled using equation 7.

The traditional PAMs have the greatest maximum stiffness, however this reduces more quickly as the joint moves away from this angle. The configuration of the sleeve PAMS also affected the maximum stiffness with the joint capable of greater torque also showing the greater stiffness.

V. Closed System Stiffness

As the volume of PAMs change with length, if the mass of air in the PAM is held constant (by not opening the valves) this will cause the pressure in the PAM to change with joint angle. This would be the case for a collision in which there is insufficient time or inadequate sensing for the control system to react.

To evaluate this property, the testing apparatus was arranged as in Fig. 3 with between 0 and 4 masses attached. The valves were controlled to move the joint to a test angle and adopt a specified stiffness. The joint was then manually displaced from the set point position by 3°, 5° or 8° during which time the valves remained closed. The change in the output torque of the joint (measured as the difference between the torque exerted by the agonist and antagonist PAMs) was approximately linear, even for larger deflections. Therefore the slope of a linear regression fitted to the torque/displacement curve yields the joint stiffness.

A sample of the results of these tests is shown in Fig. 6, representing those tests with two masses on the arm (exerting a static torque of 11Nm when the arm is at 0rad). The error bars represent the maximum deviation from the average

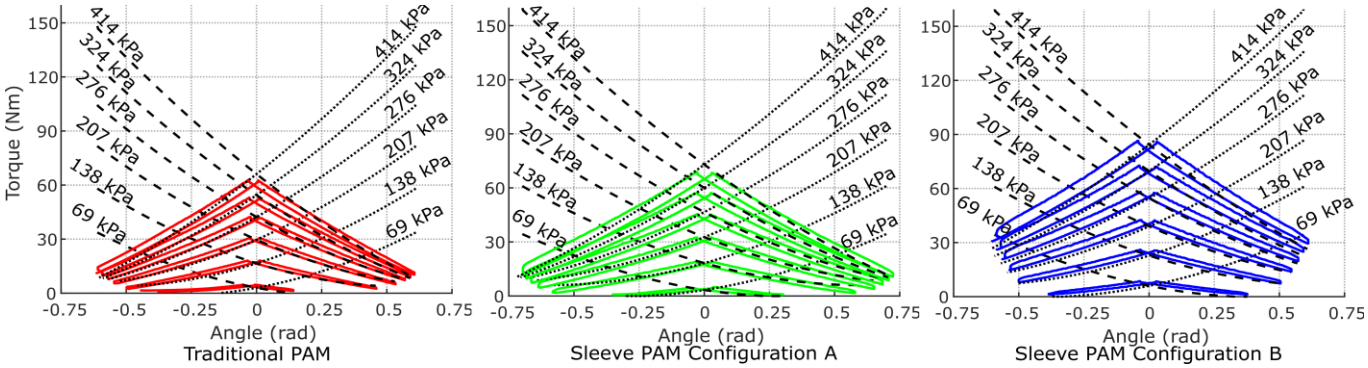

Figure 4. The torque developed by PAMs operating an antagonistically actuated joint for the case of traditional PAMs and the two sleeve PAM configurations. The dotted line is the modelled torque towards the negative angle, while the dashed line is the modelled torque towards the positive angle. The solid line represents the experimental testing in each case.

stiffness for 3°, 5° and 8° of deflection. The position set point and the direction in which the joint was displaced from the set point is also indicated. The values of stiffness recorded here are substantially greater than those in the isobaric case, particularly for the joints actuated by sleeve PAMs. It is apparent that in each case the change in pressure with rotation is greater in the B configuration of the sleeve PAM actuated joint, consequently leading to a greater stiffness for this setup.

VI. Damping

As a part of the testing procedure described for closed system stiffness, after the arm had been displaced, it was released and allowed to oscillate freely. The dynamic response allowed an assessment of damping in the system following the same approach as in [20], where a PAM actuated rotational joint, supporting a mass on an arm was modelled as a linear spring, mass, damper system. In the following calculation, the action of the two PAMs is treated as a rotational spring and damper (see Fig. 7 (a)). The system is assumed to be under damped with each oscillation resulting in a smaller amplitude than the preceding one. The logarithmic decrement of the decay is defined as

$$\delta = \ln \frac{x_1}{x_n} \tag{8}$$

where x_n is the amplitude of the n^{th} peak. As noted in [20], the equilibrium position during oscillation can be difficult to establish and so an alternative formulation utilizing the total travel between successive peaks and troughs is used instead (see Fig. 7(b))

$$\delta = \frac{2}{n\text{-}1} \ln\left(\frac{a_1}{a_n}\right) \tag{9}$$

where a_n is the n^{th} peak/trough. Using δ the damping ratio can be found using

$$\zeta = \sqrt{\frac{\delta^2}{4\pi^2+\delta^2}} \tag{10}$$

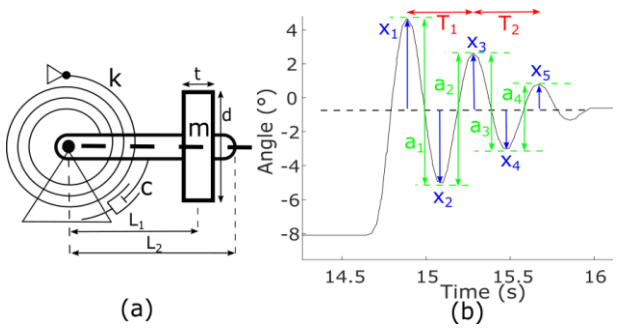

Figure 7. (a) is a representation of the actuated joint as a rotational mass spring damper system. The response of the joint actuated with two traditional PAMs after being released from an initial displacement of 9° from the 0 angle where it had a stiffnss of 88Nm/rad is shown in

For a rotational system, the viscous damping coefficient, can be related to the damping ratio by

$$c = 2\zeta\sqrt{kJ_0} \tag{11}$$

where J_0 is the moment of inertia of the arm about the pivot point. Simplifying the arm to a slender beam with a cylindrical mass attached (the massess) this is given by

$$J_0 = \frac{m_1 l_1}{3} + \left(\frac{m_2 d^2}{16} + \frac{m_2 t}{12}\right) + m_2 l_2^2 \tag{12}$$

where m_1 is the mass of the arm without the weights attached, l_1 is its length, m_2 is the mass of the weights, l_2 is the distance from the pivot to the center of the weights and t is the thickness of the weights.

The damping coefficient of the arm when two weights are applied (J_0=0.46Kg.m^2) is shown in the final row of Fig. 6. In some of these tests, particularly those with the sleeve PAMs, there were insufficient oscillations to determine δ. In all cases there were more oscillations with the traditional PAMs, improving the accuracy of these values of c. While they vary considerably, it is observed that the damping of both sleeve actuated joints is similar, while that actuated with traditional PAMs is substantially lower. Varying the joint stiffness does not have a significant effect on damping, nor does the

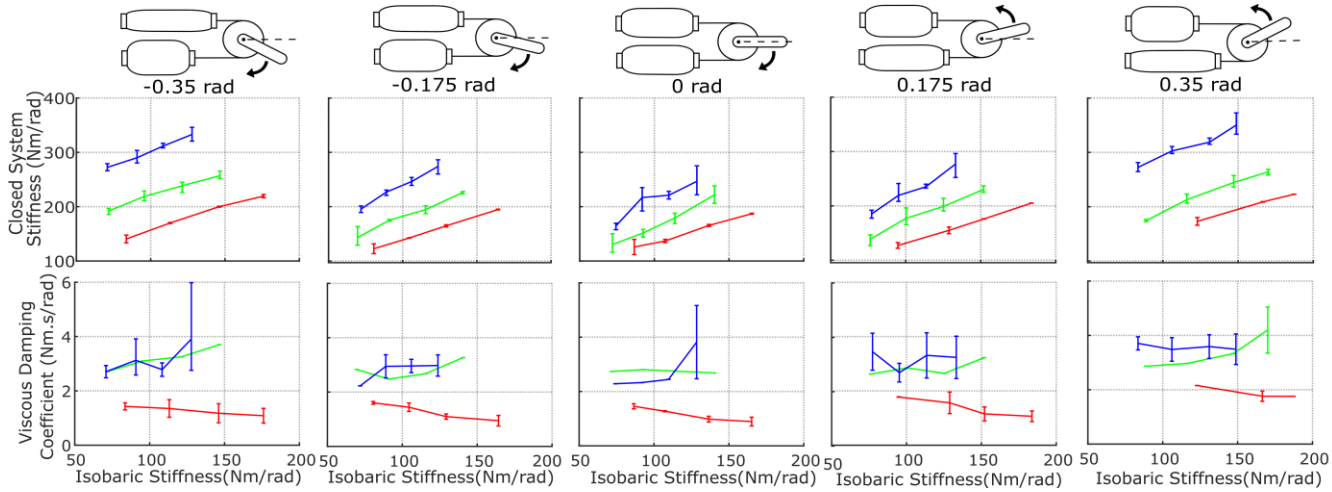

Figure 6. The results of the closed system stiffness and damping tests for the case of 2 masses (1.2 Kg each) on the arm (11Nm static torque at 0 rad). In both cases the red line represents the joint actuated with traditional PAMs while the green line shows the joint with sleeve PAMs in configuration A and the blue the sleeve PAMs in configuration B.The diagrams above the results show the direction of the forced deviation from the setpoint. The error bars illustrate the maximum and minimum values recorded.

operating angle. This is consistent with the findings in [12] which also found greater damping with the sleeve muscle which was attributed to the sliding action of the pneumatic seal.

VII. Energy Efficiency

The energy usage of the joints can be evaluated theoretically. An approach similar to that in [21] is employed, whereby an idealized compressor is the source of compressed air to a PAM. The volume of the compressor cylinder is such that it holds the mass of air, at ambient pressure, required to increase the pressure in the PAM to the pressure and contraction of interest. The energy required to drive the piston under isothermal conditions and treating air as an ideal gas is the energy required to operate the system. This analysis assumes air behaves as a perfect gas, all operations occur isothermally, and ignores dynamic effects at the joint and PAMS (G in equation 3).

While in [21] the air is first compressed before the muscle contracts isobarically using a single stroke of the compressor, here the movement of the joint is modelled in discrete steps, with a compressor stroke in each, to allow the methodology to be used for any arbitrary series of joint movements. At each step, the volume of an ideal compressor required to change the pressure in the PAM (allowing for the required changes in muscle length, volume and force output) is calculated. The model of PAM volume developed in [12] is used for this purpose. The piston then acts upon this volume of air increasing its pressure to that within the PAM. A valve linking the compressor to the PAM is then opened, and the piston completes its stroke, acting upon the total volume as the PAM length changes in response to the pressure and torque. Mathematically, the work done by the piston can be represented as:

$$W = -\int_{V_{c1}}^{V_{c2}} (P-P_{atm})dV - \int_{V_{c2}+V_{m1}}^{V_{m2}} (P-P_{atm})dV \quad (13)$$

Where P is the absolute pressure in the cylinder, P_{atm} is the ambient pressure, V_{c1} is the initial volume of the cylinder, V_{c2} is the volume after the pressure in the cylinder has been increased to that in the PAM, and V_{m1} and V_{m2} are the initial and final volumes of the muscle respectively. Making use of the ideal gas law this becomes

$$W = -\Delta m R T \ln\left(\frac{V_{c2}}{V_{c1}}\right) - P_{atm}(V_{c1}-V_{c2})$$
$$-(\Delta m+m_1)RT \ln\left(\frac{V_{m2}}{V_{c2}+V_{m1}}\right) - P_{atm}((V_{c2}+V_{m1}) - V_{m2}) \quad (14)$$

Where m_1 is the initial mass of air in the PAM and Δm is the change in this mass during the operation.

An example of the use of this methodology is shown in Fig. 8, where the stiffness of the joint is varied. In this case the joint moves in a sinusoidal motion of amplitude 0.2rad while applying a torque of 20Nm for one cycle. As the compressed air which is exhausted from the PAMs is typically lost to the atmosphere, only energy input to the PAM is considered. The joint actuated using the traditional PAM requires a greater energy input to achieve the same result. There is also considerable difference between both sleeve muscle

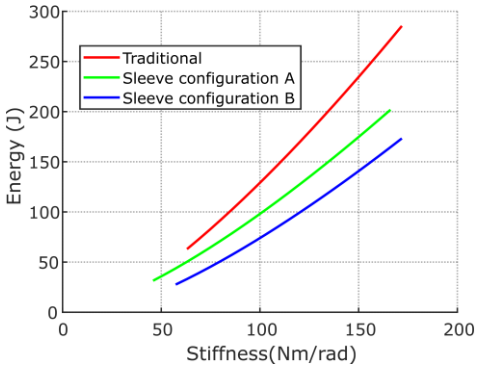

Figure 8. Energy consumption of the joint in order to move from the 0 angle sinusoidally at an amplitude of 0.2 rad, exerting 20 Nm.

configurations, with configuration A requiring the PAMs to operate in a more contracted state, thus increasing the required PAM pressure and volume and therefore energy requirement.

Due to the assumptions in this analysis, these results can only be seen as indicative of the true energy consumption. In reality the energy consumption of a compressor is complicated by temperature changes and most systems operate using a buffer tank requiring all the gas used to be pressurized to some operating pressure before being used to operate the PAMs

VIII. Conclusion

Using sleeve PAMs for antagonistically actuated joints can provide significant improvements in performance. The operating range and/or the available joint torque can be increased as demonstrated. The stiffness behavior of the joint is quite different also, especially for the case of closed system operation. This operating condition is not frequently considered in the literature, though is an important safety characteristic as it is the stiffness which will be observed upon initial impact during a collision. Here it was found that the stiffness of the sleeve PAM actuated joint can be more than three times greater than the isobaric case due the pressure change in the PAMs. This effect is less pronounced when traditional PAMs are considered as the internal PAM volume is substantially larger. Damping in the joint was found to be greater when sleeve PAMs were used. Although these tests were conducted under closed system conditions, little change was observed with stiffness and so it is likely these results are comparable to those under a broader set of operating conditions. Finally the theoretical energy consumption of the joint undertaking a simple operation was quantified. There was a significant reduction in energy use for both joint configurations using the sleeve PAMs at all stiffnesses. The procedure used here, while theoretical, may be applied to any operation to give an indication of energy consumption.

The importance of the configuration of the joint, not just in terms of pulley diameter, but also the point of rotation at which the PAMs reach full extension, is also highlighted. While only two sleeve PAM configurations were investigated, they provided substantially different operating characteristics. This is an important factor in the design of such systems and their capability.

REFERENCES

[1] A. Bicchi and G. Tonietti, "Fast and 'soft-arm' tactics: Dependability in Human-Friendly Robots," *IEEE Robotics and Automation Magazine*, vol. 11, no. 2, pp. 22–33, 2004.

[2] A. Bicchi *et al.*, "Physical human-robot interaction: Dependability, safety, and performance," *International Workshop on Advanced Motion Control, AMC*, vol. 1, pp. 9–14, 2008.

[3] M. van Damme *et al.*, "The safety of a robot actuated by pneumatic muscles-a case study," *International Journal of Social Robotics*, vol. 2, no. 3, pp. 289–303, 2010.

[4] M. Zinn, O. Khatib, B. Roth, and J. K. Salisbury, "Playing it safe: Dependability in Human-Friendly robots," *IEEE Robotics and Automation Magazine*, vol. 11, no. 2, pp. 12–21, 2004.

[5] F. Daerden and D. Lefeber, "Pneumatic artificial muscles: actuators for robotics and automation," *European Journal of Mechanical and Environmental Engineering*, vol. 47, no. 1, pp. 11–21, 2002.

[6] Festo, "DMSP Fluidic Muscle DMSP / MAS," 2016.

[7] G. Krishnan, J. Bishop-Moser, C. Kim, and S. Kota, "Kinematics of a Generalized Class of Pneumatic Artificial Muscles," *Journal of Mechanisms and Robotics*, vol. 7, no. November, pp. 1–9, 2015.

[8] S. Davis, J. Canderle, P. Artrit, N. Tsagarakis, and D. G. Caldwell, "Enhanced Dynamic Performance in Pneumatic Muscle Actuators," *Proceedings of the 2002 IEEE International Conference on Robotics and Automation*, vol. 3, no. May, pp. 2836–2841, 2002.

[9] T. Driver and X. Shen, "Sleeve Muscle Actuator: Concept and Prototype Demonstration," *Journal of Bionic Engineering*, vol. 10, no. 2, pp. 222–230, 2013.

[10] T. Driver and X. Shen, "Design and Control of a Sleeve Muscle-Actuated Robotic Elbow," *Journal of Dynamic Systems, Measurement, and Control*, vol. 136, no. July 2014, p. 041023, 2014.

[11] M. F. Cullinan, E. Bourke, K. Kelly, and C. McGinn, "A McKibben Type Sleeve Pneumatic Muscle and Integrated Mechanism for Improved Stroke Length," *Journal of Mechanisms and Robotics*, vol. 9, no. 1, p. 011013, 2017.

[12] M. F. Cullinan, E. Bourke, K. Kelly, and C. Mcginn, "Dynamic characterization and phenomenological modelling of sleeve pneumatic artificial muscles [UNDER REVIEW]," *Journal of Dynamic Systems, Measurement and Control*, 2018.

[13] D. A. Kingsley, R. D. Quinn, and R. E. Ritzmann, "A Cockroach Inspired Robot with Artificial Muscles," in *International Conference on Intelligent Robots and Systems*, 2006, pp. 659–666.

[14] M. Tavakoli, L. Marques, and A. T. De Almeida, "A comparison study on pneumatic muscles and electrical motors," in *IEEE International Conference on Robotics and Biomimetics, ROBIO 2008*, 2008, pp. 1590–1594.

[15] Marlow Ropes, "Datasheet d12 max sk75 sk78," 2017.

[16] CUI Inc., "Series : AMT20," 2016.

[17] Honeywell, "TruStability Board Mount Pressure Sensors HSC Series—High Accuracy, Compensated/Amplified," 2014.

[18] LCM Systems Ltd, "STA-1 Aluminium S Type Tension & Compression Load Cell," 2015.

[19] Matrix SpA, "Solenoid Valves 720 series 2/2 3/2," 2017.

[20] M. Sekine, R. Kokubun, and W. Yu, "Investigating the Effect of a Mechanism Combined with a Speed-Increasing Gear and a Pneumatic Artificial Muscle," *Actuators*, vol. 7, no. 2, p. 22, 2018.

[21] C.-P. Chou and B. Hannaford, "Measurement and modelling of McKibben pneumatic artificial muscles," *Robotics and Automation, IEEE Transactions on*, vol. 12, no. 1, pp. 90–102, 1996.